Journal of Integrative Agriculture 2026, 25(8): 3469–3482

Available online at ScienceDirect

Journal of Integrative Agriculture



RESEARCH ARTICLE

Understanding cropland parcel change without producing cropland parcel maps: A novel structural change detection approach

Shiyao Li[1, 2], Qiangyi Yu[2, 3#], Yulin Duan[2], Huibin Li[2], Wenjuan Li[2], Zhanli Sun[3], Daniel Müller[3, 4, 5], Baofeng Su[1#], Wenbin Wu[2]

[1] *College of Mechanical and Electronic Engineering, Northwest A&F University, Yangling 712100, China*
[2] *State Key Laboratory of Efficient Utilization of Arable Land in China/Key Laboratory of Agricultural Remote Sensing (AGRIRS), Ministry of Agriculture and Rural Affairs/Institute of Agricultural Resources and Regional Planning, Chinese Academy of Agricultural Sciences, Beijing 100081, China*
[3] *Leibniz Institute of Agricultural Development in Transition Economies (IAMO), Halle (Saale) 06120, Germany*
[4] *Geography Department, Humboldt-Universität zu Berlin, Berlin 10099, Germany*
[5] *Integrative Research Institute on Transformations of Human-Environment Systems (IRI THESys), Humboldt-Universität zu Berlin, Berlin 10099, Germany*

Highlights

- The size, shape, and distribution of cropland parcels are key features of agricultural systems.
- Traditional schemes to obtain parcel change information require wall-to-wall mapping.
- A new approach is proposed that can achieve the same purpose without mapping.
- Comparing the number of edge pixels enables efficient detection of changes in cropland parcels.

Abstract

Cropland parcels are the basic unit for agricultural production, and their size and shape may change due to human activities, e.g., land consolidation. Remote sensing has been increasingly used for mapping cropland parcel, yet detecting changes in cropland parcels by wall-to-wall mapping is time-consuming. This paper proposes a new algorithm to identify whether and where cropland parcel changes have been undertaken without generating complete parcel maps. We use the number of edge pixels derived from remote sensing imagery as a proxy indicator for cropland parcel changes. First, we apply a Sobel operator to delineate the total edge pixels of parcels from dual-time images. Second, we apply the connected-components labeling to remove pseudo-edges arising from non-cropland built structures and transmission towers. We then perform topological optimization, including morphological dilation and skeleton extraction, to eliminate redundant edge pixels for parcel structure. Finally, we detect whether parcel changes have been undertaken by counting and comparing the number of edge pixels derived from dual-time images. We applied this innovative framework in five regions in East Asia where land consolidation has significantly changed cropland parcels. Our method demonstrated robust detection results, with stable accuracy, precision, recall, and F1-score, all exceeding 0.85. Screening redundant edge pixels reduced noise and permitted efficient detection of changes in cropland parcels. Our method extends the traditional detection of semantic change to structural change and can quickly detect cropland parcel changes with high accuracy. This capability offers the potential to identify hotspot areas of cropland changes on a larger scale without the need to produce full cropland maps, which is particularly useful for monitoring land consolidation programs.

Keywords: field boundary delineation, image segmentation, change detection, land consolidation, remote sensing

Received 9 June 2025; Received in revised form 10 August 2025; Accepted 8 September 2025; Available online 27 October 2025
Shiyao Li, E-mail: shiyaoli@nwafu.edu.cn; #Correspondence Qiangyi Yu, E-mail: yuqiangyi@caas.cn; Baofeng Su, E-mail: bfs@nwsuaf.edu.cn

© 2026 CAAS. Publishing services by Elsevier B.V. on behalf of KeAi Communications Co. Ltd. This is an open access article under the CC BY-NC-ND license (http://creativecommons.org/licenses/by-nc-nd/4.0/). Peer review under responsibility of Editorial Board of *Journal of Integrative Agriculture*.
doi: 10.1016/j.jia.2025.10.014

1. Introduction

Cropland parcels serve as fundamental agricultural units (Gónzalez *et al.* 2007; Persello *et al.* 2019), determine the spatial structure of cropland (Yang *et al.* 2014; Kwinta *et al.* 2017) and are related to agricultural scale (Bey *et al.* 2020; Jänicke *et al.* 2024), machinery utilization (Janulevičius *et al.* 2019; Al-Amin *et al.* 2023), biodiversity (Clough *et al.* 2020; Noack *et al.* 2022; Li S N *et al.* 2025), and sustainability (Duan *et al.* 2021; Gao *et al.* 2024; Wang *et al.* 2025). While the size and shape of parcels are generally stable, their structure and configuration may change due to strong interventions from various biophysical, socioeconomic, and institutional factors (Qian *et al.* 2020; Gu *et al.* 2023; Hemond *et al.* 2023). For example, contemporary agricultural development is often characterized by the consolidation of smaller lands into larger parcels (Langeveld *et al.* 2006). In Germany, the average parcel size increased 3.7-fold from 1949 to 1994 due to land consolidation (LC) efforts (Hendricks *et al.* 2014). Similarly, China's Well-Facilitated Farmland Construction Programs aim to merge fragmented parcels to support mechanization and irrigation (Rogers *et al.* 2021; Yu *et al.* 2025). Therefore, understanding changes in cropland parcels is crucial for comprehending agricultural transformations shaped by land management policies, resource allocation, and broader socio-environmental dynamics (Fritz *et al.* 2015).

Remote sensing is an effective method for mapping the size, shape, and distribution of cropland parcels (Li M M *et al.* 2025). The basic idea of cropland parcel mapping is image segmentation and boundary delineation, and it is becoming more effective with the development of machine learning and the availability of high-resolution images and multimodal satellite data (Xu *et al.* 2022; Wang *et al.* 2023). For example, Xu *et al.* (2024) combined Mask RCNN and DeepSnake in a contour-based instance segmentation network to extract parcel boundaries from Google Earth imagery. Sun *et al.* (2025) developed a sample-free method that integrates super-resolution reconstruction with a dual-edge-corrected Segment Anything Model to delineate fields from Sentinel-2 or PlanetScope images. García-Pedrero *et al.* (2019) applied a convolutional neural network to delineate parcels based on open Land Parcel Information Systems (LPIS) data. Despite the current progress in parcel boundary delineation, understanding changes in cropland parcels remains a challenge. Most existing studies only mapped cropland parcels at a fixed time stage. Only few case studies have analyzed changes in the size and shape of cropland parcels by overlaying accurate cropland parcel maps from different time stages, such as analyses based on the use of existing LPIS data in Europe. However, generating time-series parcel maps remains labor-intensive, limiting timely detection of human-induced parcel changes in areas without LPIS coverage.

Change detection originated from computer vision and employs well-designed algorithms to directly generate pixel-level differences (Feng *et al.* 2015; Huang *et al.* 2020; Huang *et al.* 2022). Traditional methods like image differencing and ratioing lay the foundation by capturing pixel-level spectral differences but are sensitive to noise and environmental interference (Singh 1989). With the rise of machine learning, supervised methods such as support vector machine (SVM) for change detection have improved accuracy by learning from labeled change samples, yet they rely heavily on high-quality training data (Hussain *et al.* 2013). In recent years, deep learning has brought new advancements. Models like U-Net and its variants achieve end-to-end change detection by extracting deep features, showing strong performance in complex scenes (Shi *et al.* 2020). However, these methods mainly focus on semantic changes between different land cover types. For example, Sun *et al.* (2024) proposed a lightweight CNANet model that semantically labels non-agricultural pixels in cropland to detect land cover type changes associated with cropland non-agriculturalization. In contrast, structural changes in land cover, such as parcel changes within cropland, require a more detailed analysis of pixel connectivity and spatial arrangement within the same land cover type (Alcantarilla *et al.* 2018). Existing methods for semantic change detection treat each land cover type as a uniform label, which overlooks the fine-grained pixel-level patterns essential for detecting structural changes (Liu *et al.* 2019; Zhang *et al.* 2022). For instance, the implementation of LC may involve merging or splitting parcels, leading to changes in cropland parcels. However, the overall cropland area may remain stable even when the internal structure of the cropland is altered. In this case, detecting changes in cropland parcels requires analyzing pixel connectivity and distribution to identify transformations in internal structures. This underscores the challenge of adapting conventional change detection approaches to effectively understand the process of cropland parcel changes, as it involves both pixel-level differences and the spatial organization of these pixels within a given type.

In order to quickly identify the hotspots of cropland parcel changes caused by land consolidation (LC), we propose a novel and efficient approach for quantifying cropland parcel changes without relying on wall-to-wall parcel maps. Instead of focusing on the semantic information of all pixels – the way traditional land cover change detection analysis basically relies on – we focus on edge pixels as they represent the abrupt changes in grayscale value between adjacent pixels and are frequently used as the basic input in image segmentation for cropland boundary delineation. Counting the edge pixels inside a fixed window provides a direct proxy for parcel geometry: the total rises when parcels are small and fragmented and falls when neighbouring parcels are merged into larger, simpler fields, because boundary length per unit area contracts accordingly (Garcia-Pedrero *et al.* 2015). Within LC areas, changes in edge pixel count predominantly indicate parcel merging or splitting. Soil exposure or temporary fallow rarely triggers large gray-level discontinuities, so such factors do not materially alter the edge pixel signal. Therefore, by counting the number of edge pixels, we can easily obtain a quantitative assessment of whether the focused area has undergone significant modifications in the cropland boundary. The advantages of our method become apparent when compared to traditional cropland parcel mapping methods. Our approach is more error-tolerant and labor-saving. Leveraging these strengths,

we treat the total number of edge pixels within a fixed window as a structural proxy for parcel change and hypothesise that temporal shifts in this proxy reveal parcel-scale restructuring. We test the approach in five East-Asian regions where LC has demonstrably enlarged and simplified fields, evaluating whether the proxy can highlight change hotspots without producing a single parcel map and thereby offer a scalable tool for regional-to-national LC monitoring.

2. Materials and methods

2.1. A new framework to understand cropland parcel change without mapping

The traditional scheme for understanding cropland parcel change follows a multi-step wall-to-wall mapping workflow. It usually begins with manual annotation of cropland pixels to build a training set, continues with model training and parcel segmentation, and ends with accuracy assessment. Because this entire sequence must be executed for every image in the time series, it is computationally demanding, sensitive to segmentation error, and heavily dependent on labour-intensive labels (Fig. 1). Crucially, the edge pixels that lie along the cropland–non-cropland interface already delineate parcel boundaries and therefore concentrate the structural information needed for change analysis.

Leveraging this insight, we introduce a lightweight alternative that eliminates wall-to-wall mapping. The framework treats the number of edge pixels within a fixed analysis window as a structural proxy for detecting cropland parcel change. By directly comparing proxy values between dates, parcel-scale dynamics are identified without parcel segmentation, map validation, or cross-temporal overlay (Fig. 1). This approach removes the most labour- and computation-intensive stages of the conventional workflow while retaining sensitivity to parcel-level change.

2.2. Study area

LC serves as an effective land management strategy that enhances agricultural production (Abubakari *et al.* 2016), contributing to food security, modern agriculture, and sustainable development (Jiang *et al.* 2022). Cropland parcels after LC are characterized by centralized and contiguous parcels of regular shape while prior to LC, parcels were smaller and exhibited varied shapes, including regular (rectangular, square) and irregular forms (narrow, fragmented). These shape variations represent a key source of instability for the methodology proposed in this study. To test the proposed edge pixel-based change detection method, we selected five regions across East Asia, specifically in Central, North, East, and Southwest China, as well as Hokkaido, Japan. These sites reflect distinct geographical characteristics, diverse parcel shapes, and significant structural changes due to LC, where irregular, small-scale parcels have been consolidated into larger, more regular ones (Fig. 2).

In Central China, we selected Jingzhou City in Hubei Province. The original cropland units were predominantly rectangular parcels with blurred edge characteristics. The LC project, covering approximately 1.19 km^2, was implemented from 2017 to 2018, reducing parcel numbers from 389 to 167. In Tangshan City, Hebei Province, in North China, the original cropland pattern consisted of neatly arranged fine square parcels with clear boundaries and uniform internal texture. The LC project also covered 1.19 km^2, was initiated in 2017 and completed in 2018, and similarly resulted in a reduction of the number of parcels from 389 to 167. The test site in East China in Lu'an City, Anhui Province, features a complex cropping structure. Following an LC project from 2019 to 2020 covering 1.85 km^2, scattered parcels were consolidated into contiguous units, reducing parcel counts from 917 to 283. The test site in Southwest China, Xigaze

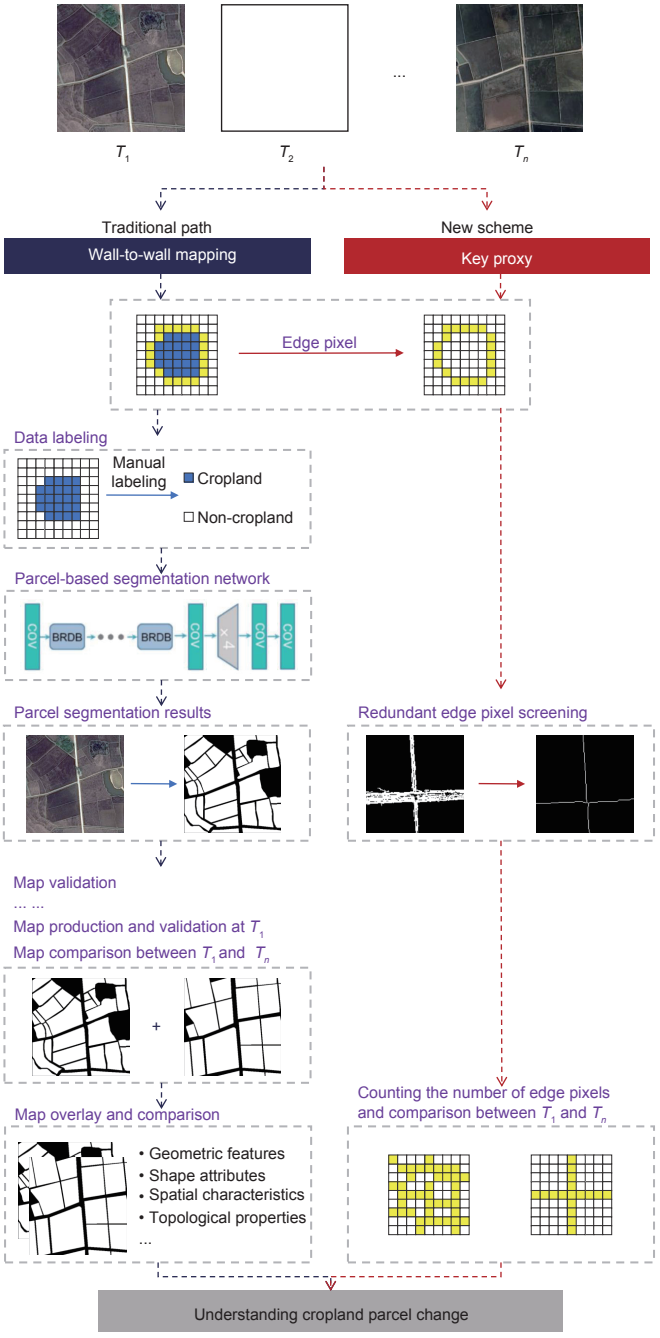


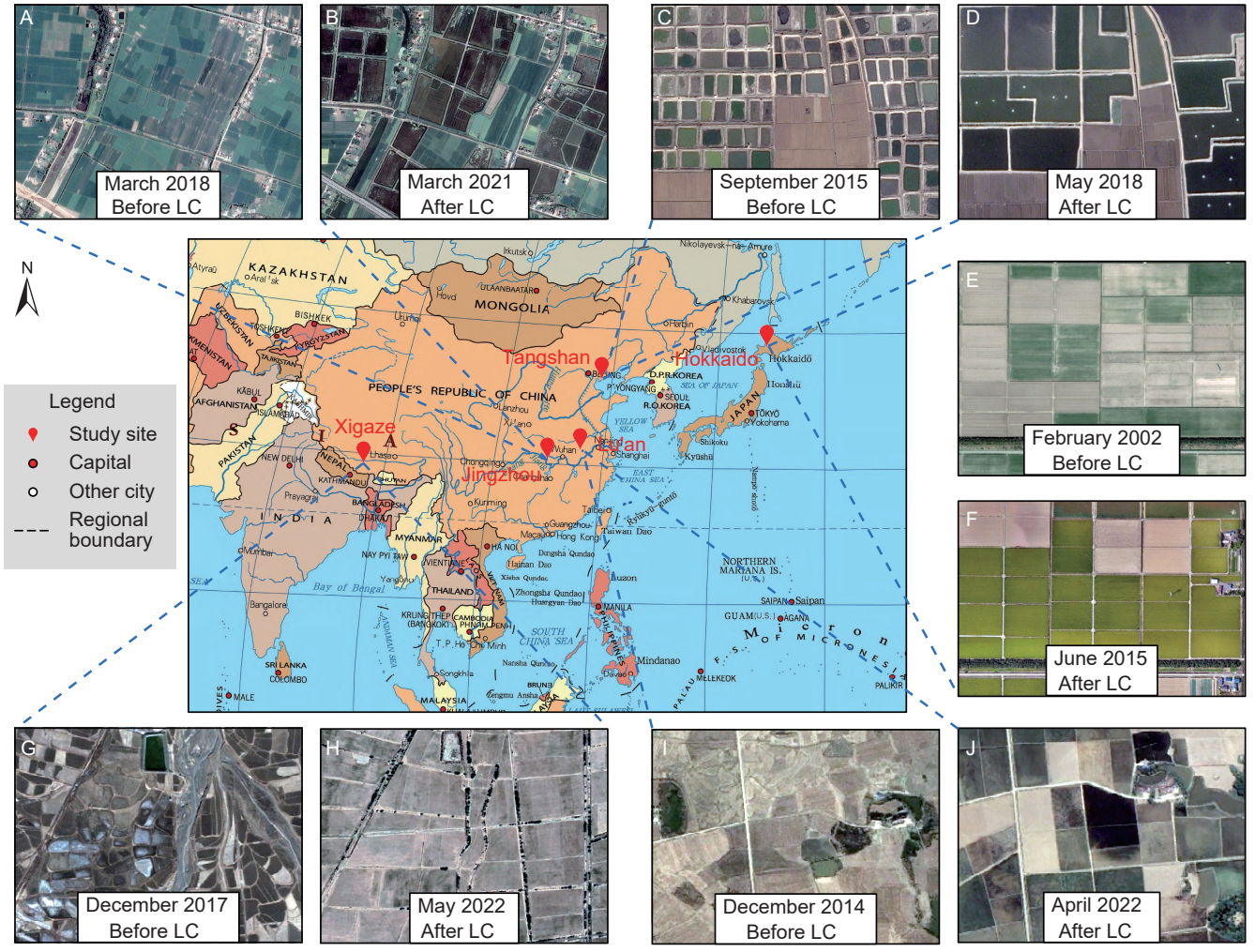
Fig. 1 Comparison of traditional and new schemes for understanding cropland parcel change.

City, Xizang Autonomous Region, contained a mix of narrow and irregular parcels with clearly defined boundaries. An LC project spanning 2.79 km^2 was completed from 2020 to 2021, decreasing the parcel count from 498 to 98. The Hokkaido test site in Japan reflects a unique approach to LC, focusing on the further consolidation of already regularized cropland. The project, conducted from 2003 to 2004, reduced the number of parcels from 157 to 90 within an area of 0.95 km^2.

2.3. Data

We employed Google Earth Pro imagery with a spatial resolution of 0.53 m and three RGB bands. The data are freely available, enhancing the universal applicability of our method. To detect parcel-scale restructuring effectively, multi-temporal imagery is indispensable for capturing changes in surface conditions before and after LC. At each study site, we collected multi-temporal imagery with at least three acquisition dates, comprising both changed parcels (before and after LC) and unchanged parcels (within the same period), thereby establishing a robust dataset for cropland parcel change detection. Given that LC implementation occurred at different times across sites, it was not feasible to standardize the image acquisition dates. Instead, we determined the LC implementation periods using official documents and literature, and subsequently collected all high-quality, cloud-free images that adequately covered the corresponding time spans. To minimize the impact of phenological variation, the dataset includes both intra-season and cross-season image pairs to test robustness. The complete data list is presented in Table 1.

All study sites are cropland-dominated, and LC projects scarcely change land-cover categories; instead, they reshape cropland boundaries through parcel merging and splitting. Non-cropland features (roads, water bodies, settlements, forests) remain virtually static during the observation window and therefore contribute negligible temporal fluctuation to edge pixels. After radiometric correction and co-registration, each image was cropped to 512×512 pix tiles focusing exclusively on cropland areas. In total, we obtained 625



审图号：GS 京 (2026) 0965 号

Fig. 2 Location of study sites and Google Earth images before and after land consolidation (LC). A and B, Google Earth images of Jingzhou study site before and after LC. C and D, Google Earth images of Tangshan study site before and after LC. E and F, Google Earth images of Hokkaido study site before and after LC. G and H, Google Earth images of Xigaze study site before and after LC. I and J, Google Earth images of Lu'an study site before and after LC.

Table 1 Acquisition dates of Google Earth images

Site	Before land consolidation	After land consolidation
Jingzhou	April 2014	March 2021
	July 2017	
	March 2018	
Tangshan	September 2007	May 2018
	October 2013	September 2022
	September 2015	May 2024
Lu'an	April 2017	May 2022
	December 2017	
	March 2019	
Xigaze	December 2011	April 2022
	September 2013	
	December 2014	
	May 2018	
Hokkaido	May 2002	June 2015
	May 2003	April 2019

image slices, with 935 pairs of both parcel-changed and parcel-unchanged image pairs. We randomly divided the samples into a training (280 pairs) and a test set (655 pairs). The training set, labeled with changed and unchanged scenarios of cropland parcels, was used to train the SVM classifier, while the test set was used to evaluate the algorithm's feasibility.

2.4. Methodology

The core idea of the edge pixel-based method is that the number of edge pixels will decrease when small parcels are consolidated into larger ones. To ensure the reliability of edge pixels as a basis for change detection while avoiding wall-to-wall mapping, we employ a lightweight three-step approach: total edge pixel delineation, redundant edge pixel screening, and cropland parcel change detection (Fig. 3). In the proposed three-step workflow, decisions are based solely on the bi-temporal variation in edge pixel counts; the algorithm bypasses traditional image segmentation, vectorization, and parcel delineation. Accordingly, we omit explicit boundary extraction and accuracy assessment, as the goal is to identify whether a structural change has occurred, not to reconstruct exact field boundaries. By removing the labor-intensive mapping stage, the pipeline avoids error propagation from boundary delineation and remains lightweight and computationally efficient.

Total edge pixel delineation To extract the edge of cropland parcels, we process the bi-temporal remote sensing image gray-scale for feature extraction. The brightness information in gray-scale images often contains important information about image structure and texture. The edge detection methods do not require pixel-by-pixel segmentation, making them more suitable for identifying a wide range of edges with low precision in remote sensing images. The Sobel operator is employed for edge detection, connecting neighboring pixels based on gradient information to smooth out discontinuous edges (Sobel 1978; Tong *et al.* 2011; Ranjan *et al.* 2023). The Sobel operator is a discrete, first-order

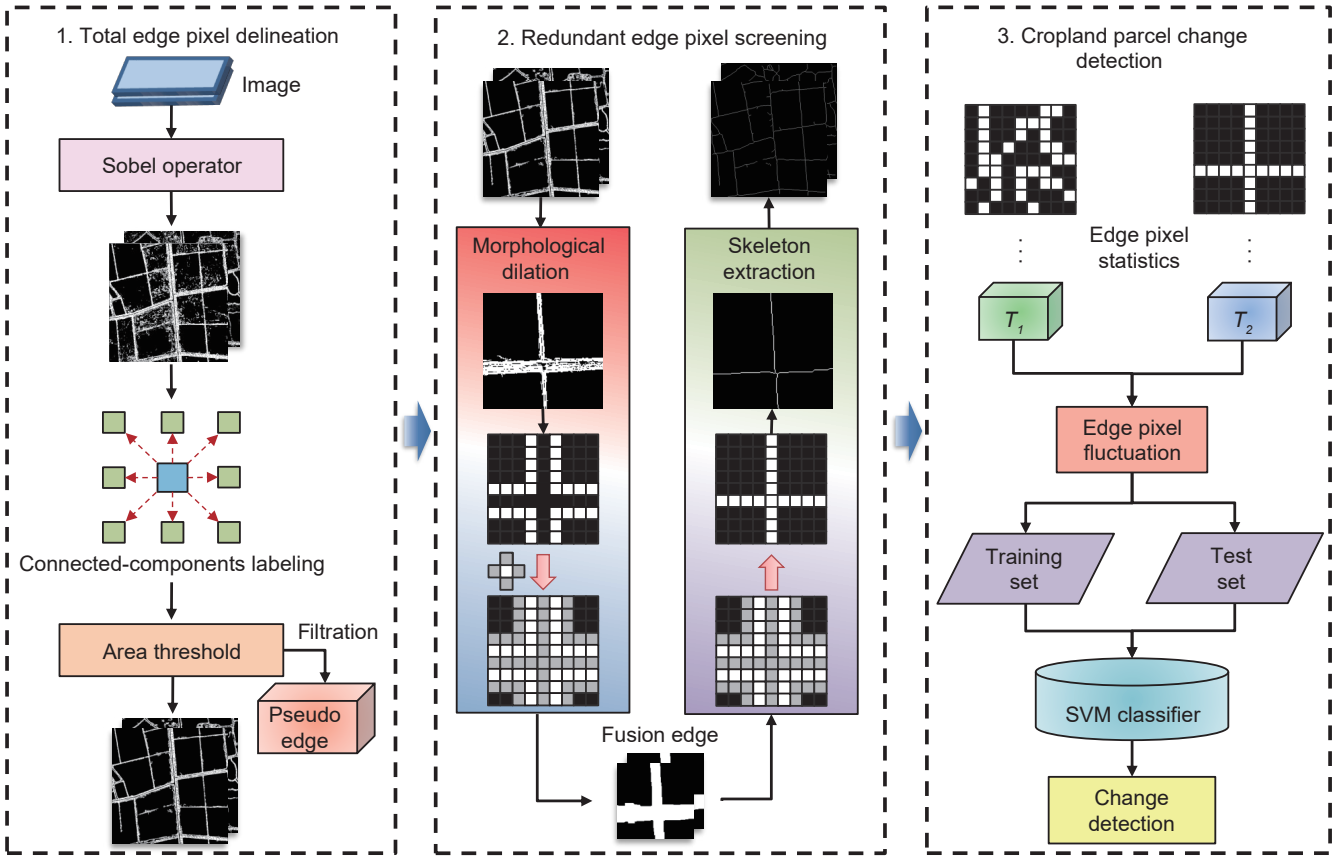


Fig. 3 Workflow of cropland parcel change detection based on edge pixels.

differential operator for edge detection, involving Gaussian smoothing and differential derivation (Tong *et al.* 2011; Kong *et al.* 2023). In comparison to other complex operators with high accuracy, the Sobel operator strikes a better balance between processing speed and accuracy (Qu *et al.* 2005). The fundamental concept involves using two different convolution checks for images horizontally and vertically in the convolution operation, followed by image edge detection through first-order differential calculation (Sobel 1978; Qu *et al.* 2005).

Assuming that the input image is $I(x, y)$, the convolution template of the Sobel operator for horizontal G_x and vertical G_y is as follows:

$$G_x=\begin{bmatrix}-1 & 0 & 1\\ -2 & 0 & 2\\ -1 & 0 & 1\end{bmatrix} \quad G_y=\begin{bmatrix}-1 & -2 & -1\\ 0 & 0 & 0\\ 1 & 2 & 1\end{bmatrix} \tag{1}$$

For the input image I, the horizontal gradient g_x and vertical gradient g_y are computed using the Sobel operator:

$$g_x=I\times G_x \quad g_y=I\times G_y. \tag{2}$$

where × represents a convolution operation.

The gradient magnitude M and gradient direction θ are calculated by the following equations:

$$M=\sqrt{g_x^2+g_y^2} \tag{3}$$

$$\theta=\arctan(\frac{g_y}{g_x}) \tag{4}$$

The employment of these two thresholds could enhance edge selectivity. The gradient threshold regulates the edge intensity, ensuring that only a sufficiently substantial gradient is recognized as an edge. The angle threshold permits some deviation in direction to be accepted to a certain extent, facilitating the connection of edges in various directions.

Despite initial edge detection using the Sobel operator, the imagery still contains two distinct edge categories: structural edges, which exclusively delineate cropland parcel boundaries (including field ridges and inter-parcel roads), and pseudo-edges, which arise from non-structural factors. The pseudo-edges can be further classified into four types: (1) illumination artifacts, such as shadow boundaries caused by solar angle variations; (2) agricultural textures, including parallel furrow patterns from mechanized farming and spectral variations across crop growth stages; (3) vegetation transitions, resulting from density differences in non-parcel vegetation; and (4) non-agricultural features, such as field buildings and transmission towers. To isolate valid parcel boundaries, we used the connected-components labeling method to detect connected regions in the binary edge graph and label them. Common connected domains are typically categorized into two types: four-connected domains and eight-connected domains (He *et al.* 2017). We adopted an eight-connected region, which involves examining whether there are adjacent edge pixels in the eight directions around a given edge pixel. Since structural edges tend to form continuous, spatially coherent boundaries, while pseudo-edges often appear as fragmented or isolated patterns, this connectivity constraint allows for the identification of coherent edge structures. Within a connected domain, every pair of points is linked, and no two connected regions overlap (Rosenfeld *et al.* 1966; Walczyk *et al.* 2010). By calculating the size of each connected region, we filter out small, disjoint pseudo-edges based on an area threshold, ensuring that only connectivity components representing parcel boundaries are retained. We then computed the area of each component and discarded those smaller than 50 pixels — the threshold that yielded the optimum noise-to-signal ratio in a sweep from 20 to 100 pixels — thereby retaining only components that faithfully delineate parcel boundaries.

Redundant edge pixel screening Although most pseudo-edges have been eliminated from the edge detection results in the previous stage, there are still many redundant edges for the parcel topology. A parcel topology requires only one edge, while a ridge includes multiple feature edges within it. Therefore, morphological operations are pivotal in enhancing and simplifying the edges detected in the previous stage. The spatial extent of all edges is enlarged by morphological dilation processing to fuse all edges on the parcel topological structure (Meng 2018). The outcome of the dilatation operation is to combine the background pixels in contact with the image boundary into the image, which can fill relatively small holes in the image and small dents at the edge of the image. The dilatation operation of binary image $I_1(x, y)$ is shown in eq. (5).

$$I_2(x,y)=max_{(s,t)\in E}\{I_1(x-s,y-t)\} \tag{5}$$

where $I_2(x, y)$ is the pixel value in the dilatated image whose coordinate is (x,y), E is the convolution kernel of the dilatation operation, and (s,t) is the coordinate in the convolution kernel.

The subsequent stage involves extracting the skeleton from the fused edges. Skeleton extraction algorithms refine a connected region to a width of one pixel for feature extraction and target topology representation (Lam *et al.* 1992). Through the continuous traversal of the specified connection area in the image, the boundary pixels are identified and removed in each traversal, ensuring that the connection of the subject area is not damaged (Al Smadi *et al.* 2021). Commonly used skeleton extraction methods include thinning algorithm (Chen *et al.* 2012), the Zhang-Suen thinning algorithm (Zhang and Suen 1984), the Lee thinning algorithm (Lee *et al.* 1994), and the medial axis transformation algorithm (Choi *et al.* 1997). The Zhang-Suen thinning algorithm demonstrates superior performance in preserving the main topology, as it effectively eliminates redundant branches and ensures a complete and smooth overall skeleton (Fig. 4). Hence, we adopt the Zhang-Suen thinning algorithm.

The Zhang-Suen thinning algorithm adopts a two-layer cycle structure to scan and detect the pixels and then eliminate the edge pixels. Fig. 5 illustrates the Zhang-Suen thinning algorithm for an eight-neighbor connectivity map.

Step 1: The target pixel P1 should meet the exclusion conditions:

(1) $2\le N(P1)\le 6$

(2) $S(P1)=1$

(3) $P2\times P4\times P6=0$

(4) $P4\times P6\times P8=0$

where N(P1) is the number of nonzero points in {P2, ... , P9}; and S(P1) is the number of 1–0 patterns in the ordered set {P2, ... , P9}.

Step 2: Simply adjust the third and fourth conditions in the first level of the loop to the following equation, as follows:

(1) 2≤N(P1)≤6
(2) S(P1)=1
(3) P2×P4×P8=0
(4) P2×P6×P8=0

If the target pixel P1 meets the two-layer loop condition, then it can be deleted. Otherwise, the pixel is retained (Zhang *et al.* 1984).

With the skeleton extraction algorithm, the fused edges are converted into skeleton structures, and these edges are streamlined based on topological relationships to preserve the edge's topological structure representing the shape of parcel.

Cropland parcel change detection Counting edge pixels represents the core of cropland parcel change detection. After skeletonisation, we enumerate topological edge pixels within each fixed $M\times M$ window for two acquisition dates and compute their bi-temporal fluctuation:

$$\Delta N=N_{t2}-N_{t1} \quad (6)$$

which quantifies parcel-level structural variation. Each window is labelled changed or unchanged from reference data, and ΔN serves as the sole input feature to a support-vector machine (SVM). The SVM uses an RBF kernel with hyper-parameters tuned *via* grid search and five-fold cross-validation: C=10, γ=0.01, and class_weight='balanced' to counter class imbalance. Hyper-parameters are selected *via* five-fold cross-validation, and the optimised model is applied to the test set to determine whether cropland parcels have changed, thereby obviating image segmentation, map validation, and cross-temporal overlay analysis.

Outcome evaluation We select four metrics for quantitative assessment: accuracy, precision, recall, and F1-score. Specifically, the above evaluation metrics are calculated as follows:

$$\text{Accuracy}=\frac{TP+TN}{TP+TN+FP+FN} \quad (7)$$

$$\text{Precision}=\frac{TP}{TP+FP} \quad (8)$$

$$\text{Recall}=\frac{TP}{TP+FN} \quad (9)$$

$$\text{F1-score}=2\times\frac{\text{Precision}\times\text{Recall}}{\text{Precision}+\text{Recall}} \quad (10)$$

In the above formulas, TP and TN denote the number of accurate predictions for positive and negative samples, respectively. FP and FN represent the number of false predictions for positive and negative samples, respectively.

3. Results

3.1. Total edge pixels

The results show that our method outperformed the Canny algorithm in detecting edges across both regular (rectangular, square) and irregular (narrow, broken) parcel shapes (Fig. 6). Additionally, it was observed that for rectangular parcels, square parcels, narrow parcels, and broken parcels before LC, the main factor affecting the edge detection effect was the discontinuous edge problem, which hindered the extraction of closed-edge parcels. As for the concentrated and regular-shaped parcels after LC, the fine pseudo-edge was the primary challenge interfering with the edge detection effect. Our method excelled in addressing both discontinuous and fine-grained edges, surpassing the capabilities of the Canny algorithm. Furthermore, our method effectively filtered out fine pseudo-edges, enhancing the effectiveness of cropland edge detection (Fig. 7). While a significant number of pseudo-edges had been eliminated from the edge detection results, there remained some redundant edges for the parcel topology that still required optimization (Fig. 8).

3.2. Refined edge pixels

In the second stage of our study, we simplified the edges based on topological relations to maintain the edge topological structure, which could depict the shape characteristics of the parcels and screen redundant edges. The analysis focused on the spatial relationships and connectivity among these edges, providing insights into the complex structures within cropland landscapes. Fig. 9 presented the fusion results of parcel edges in the bi-temporal images, along with the topological edges extracted from the fusion results. Following the morphological expansion operation, the spatial extent of all edges was enlarged, causing all redundant edges on a parcel topology to merge into a single edge. Then, the inflated edges were simplified to a single pixel by Zhang-Suen thinning algorithm (Zhang *et al.* 1984), which was the most essential edge capable of representing the structural feature of the parcels. The red and yellow labels in Fig. 9 marked the edge pixels statistics with and without topology optimization, showing a substantial screening of redundant edge pixels based on topology optimization operations. The cumulative operation of morphological dilation and skeleton

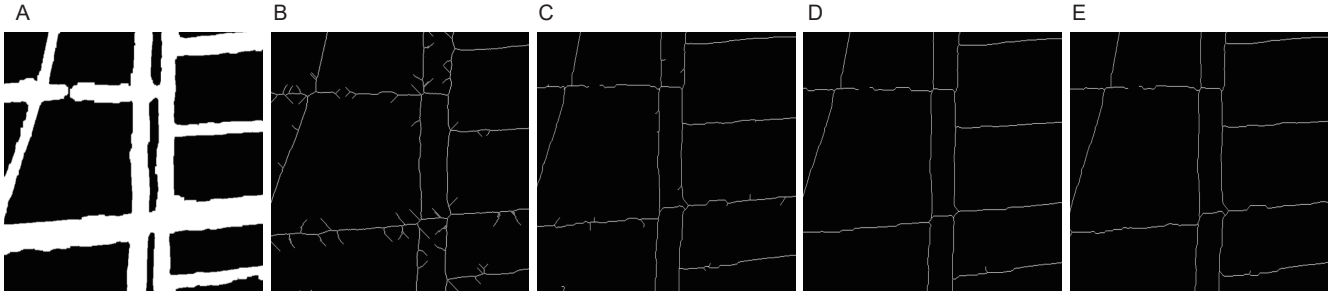


Fig. 4 Experimental results of cropland skeleton extraction. A, original mask. B, medial axis transformation. C, thinning algorithm. D, Lee thinning algorithm. E, Zhang-Suen thinning algorithm.

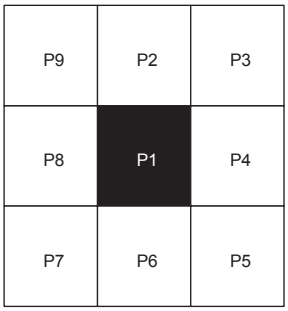


Fig. 5 Zhang-Suen thinning algorithm for eight-neighbor connectivity map. P1 is the target pixel, P2–P9 are its eight-neighborhood pixels.

extraction effectively simplifies edge complexity and highlights the structural features of the parcels.

Accurate extraction of edge features is critical for successful edge pixel-based change detection. Traditional edge detection methods failed to accurately characterize the distribution of feature contours and were susceptible to noise and pseudo-edges. We compared the significance of the difference between filtered and unfiltered edge pixels using *t*-test (Table 2). The results indicated that edge pixels without screening was unable to support change detection. There was no substantial variance in the number of edge pixels between the bi-temporal images ($P>0.05$), rendering it unsuitable as a change detection criterion due to the inclusion of numerous redundant edges in the detection results. In contrast, the edge pixels after screening effectively represented parcel structural characteristics, revealing a significant difference between bi-temporal images ($P<0.01$) that facilitates robust parcel change detection.

3.3. Cropland parcel change detection

The refined edge pixels show significant fluctuation and contrast before and after changes, enabling the detection of cropland parcel changes based on edge pixel counts (Fig. 10). We trained the SVM classifier based on the edge pixel fluctuation values from 280 image pairs in the training set, including 203 pairs in Lu'an, 31 pairs in Jingzhou, 22 pairs in Tangshan, 69 pairs in Xigaze, and 56 pairs in Hokkaido. The performance of the proposed method was evaluated on a test set (Table 3). The results demonstrate stable change detection across the dataset, with accuracy, precision, recall, and F1-scores all exceeding 0.85. The proposed method showed robust performance across various parcel shapes, including regular parcel shapes such as rectangular and square, as well as irregular parcel shapes, such as narrow and broken, thus eliminating potential sources of instability.

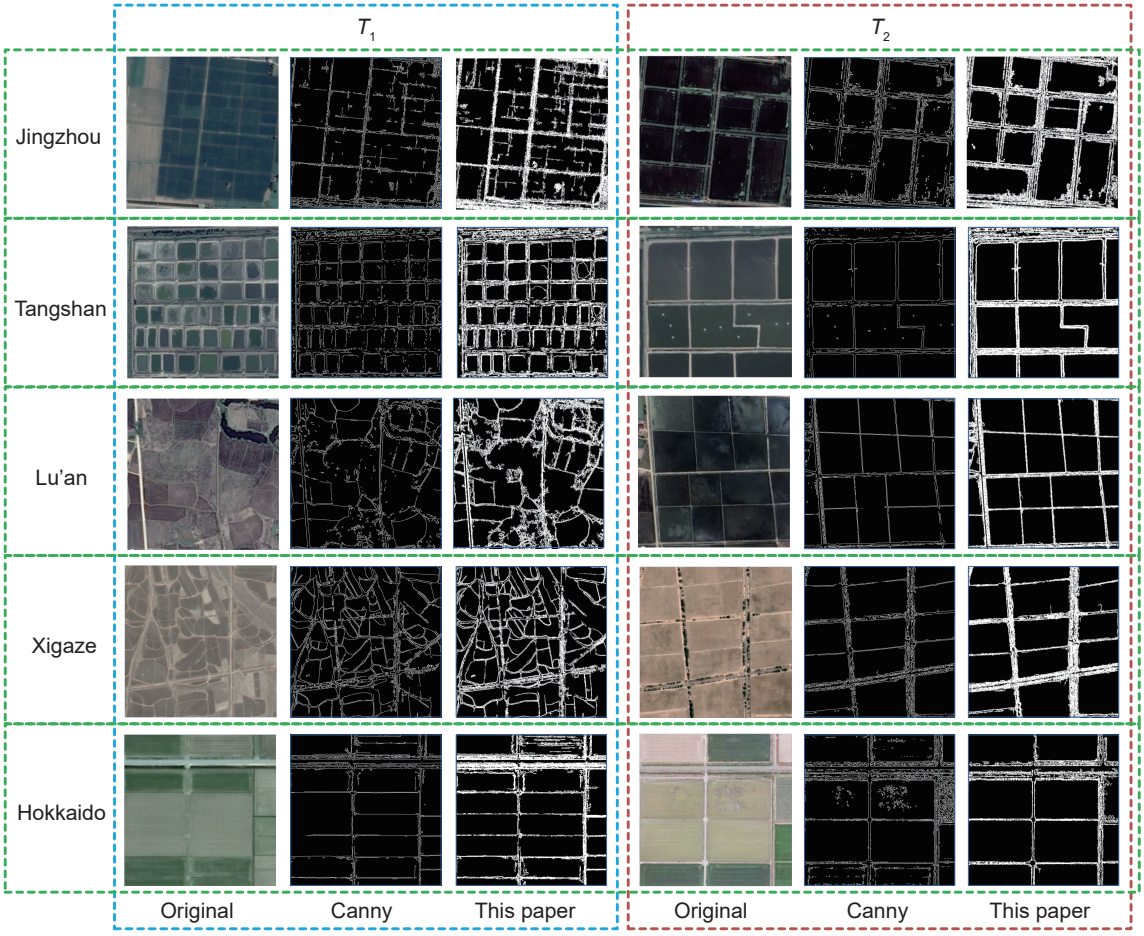


Fig. 6 Bi-temporal images cropland parcel edge detection results.

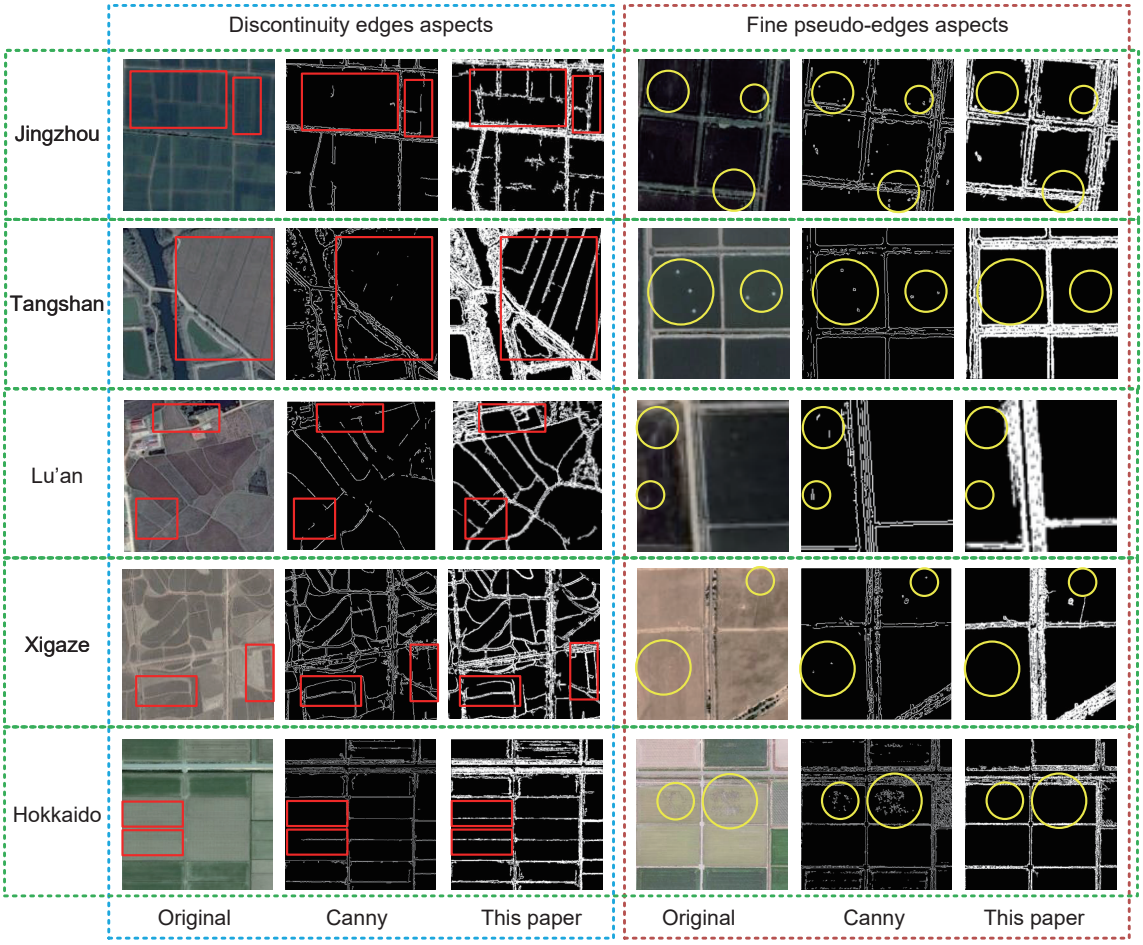


Fig. 7 The performance of two algorithms in dealing with discontinuous edges and fine pseudo-edges.

Among the study sites, Xigaze achieved the highest performance, with accuracy, precision, and F1-score each exceeding 0.95, attributed to its distinct parcel boundaries. In contrast, Lu'an exhibited slightly lower performance, which was linked to ambiguous boundaries despite meeting detection requirements. Both sites featured complex parcel structures before LC, yet the clarity of parcel edges played a more significant role in detection accuracy than parcel shape. In Hokkaido, Japan, a region where cropland regularization was further consolidated, the method also achieved stable excellent results, with accuracy, precision, recall, and F1-scores exceeding 0.90 (Table 3). These findings underscore the method's robustness and reliability in detecting structural changes, including the further consolidation of regularized parcels, across diverse agricultural landscapes.

4. Discussion

4.1. Using semantic information for structural change detection

The applications of cropland change detection have become increasingly diverse, extending beyond the scope of semantic change detection. During LC, the merging of smaller parcels into larger ones represents a marked transformation of the spatial structure, while the land cover remains unchanged. Traditional semantic change detection methods uniformly label each land cover type, capturing only spectral differences between types and overlooking internal structural details. Therefore, these methods fall short of detecting structural information. We employed structural change types within a given window as semantic labels, treating edge pixels as detection targets, which enriches semantic change detection with structural changes. Graesser *et al.* (2017) demonstrated the effectiveness of edge-based methods by estimating cropland at a parcel level using multi-temporal Landsat imagery over a large and complex agricultural region in South America. Despite these advancements, few studies have leveraged edge features specifically for structural change detection. Our method seeks to innovate in this area, using edge features to enable more precise and reliable detection of structural changes in agricultural parcels.

4.2. Linking edge pixel with field size

The pattern of cropland parcels determines the average field size in a given area, which has been regarded as a useful indicator for measuring agricultural development and resource management (Jänicke *et al.* 2024). Traditionally, data on field size is typically obtained from agricultural censuses or household surveys. Both are challenging and expensive to collect; thus infrequently available, and the temporal and spatial resolution of the statistical data is very coarse (Lowder

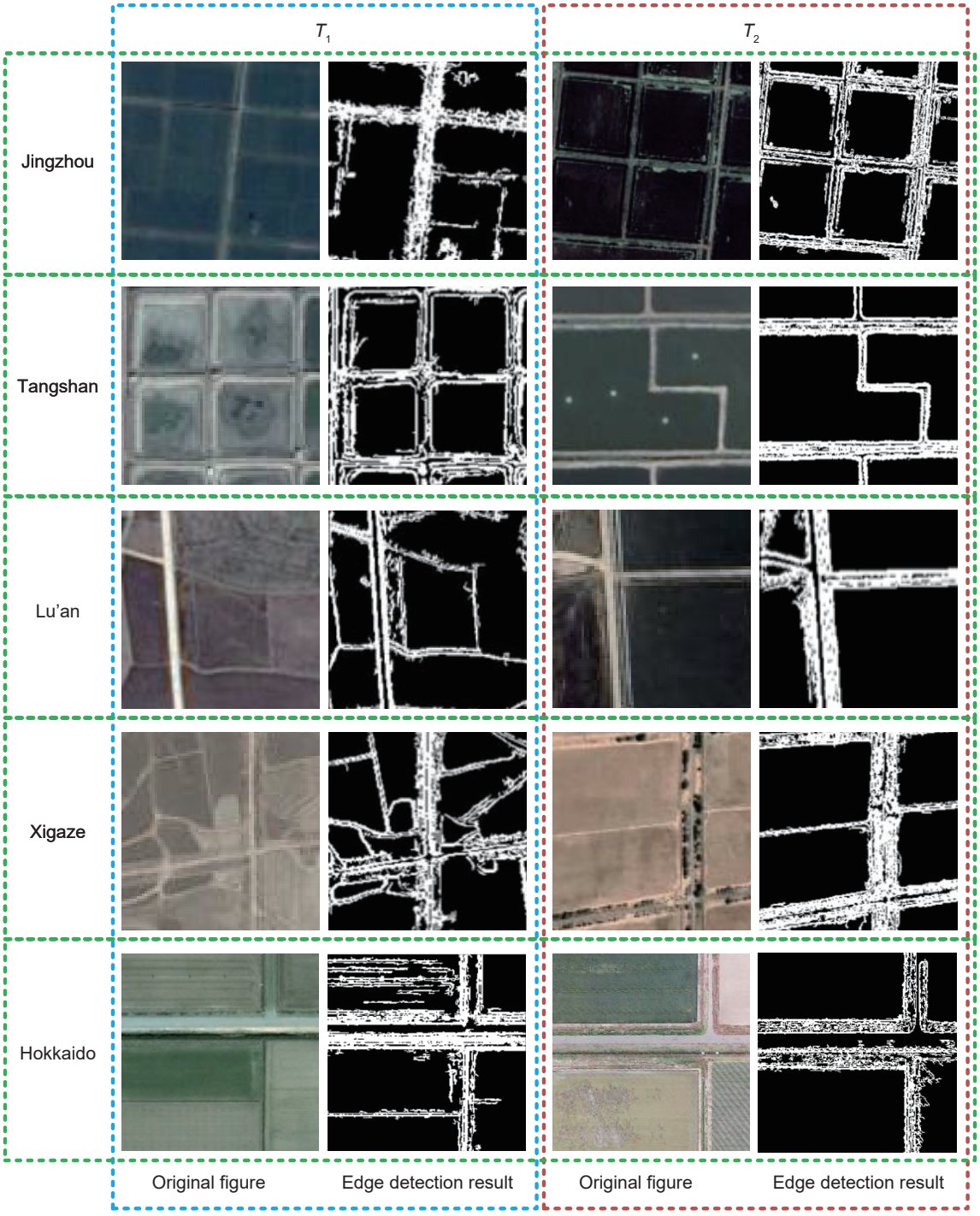


Fig. 8 Redundant edges on a parcel topology.

et al. 2021). As shown in Fig. 11, through our continuous optimization for edge pixels, the refined edge pixels showed a ratio similar to the pattern between the average perimeter and area of the field. This implied that the pattern of refined edge pixels may closely resemble field size. Du *et al.* (2024) developed a field size measurement algorithm based on medium and high-resolution satellite imagery. They used the proportion of edges per unit area of cropland to reflect field size, demonstrating the feasibility of an edge-based algorithm to estimate field size. However, in small-scale farming areas, parcels are smaller and more fragmented, and the boundaries between parcels are thinner, often less than 10 m, below the spatial resolution of common medium and high-resolution remote sensing imagery. Therefore, field size measurement in small-scale farming areas is very difficult. Our method is independent of field size and can provide field size measurements in small-scale farming environments. It is worthwhile for future studies to explore the spatial-temporal patterns of field size on a large scale, based on the negative relationship between field size and the number of edge

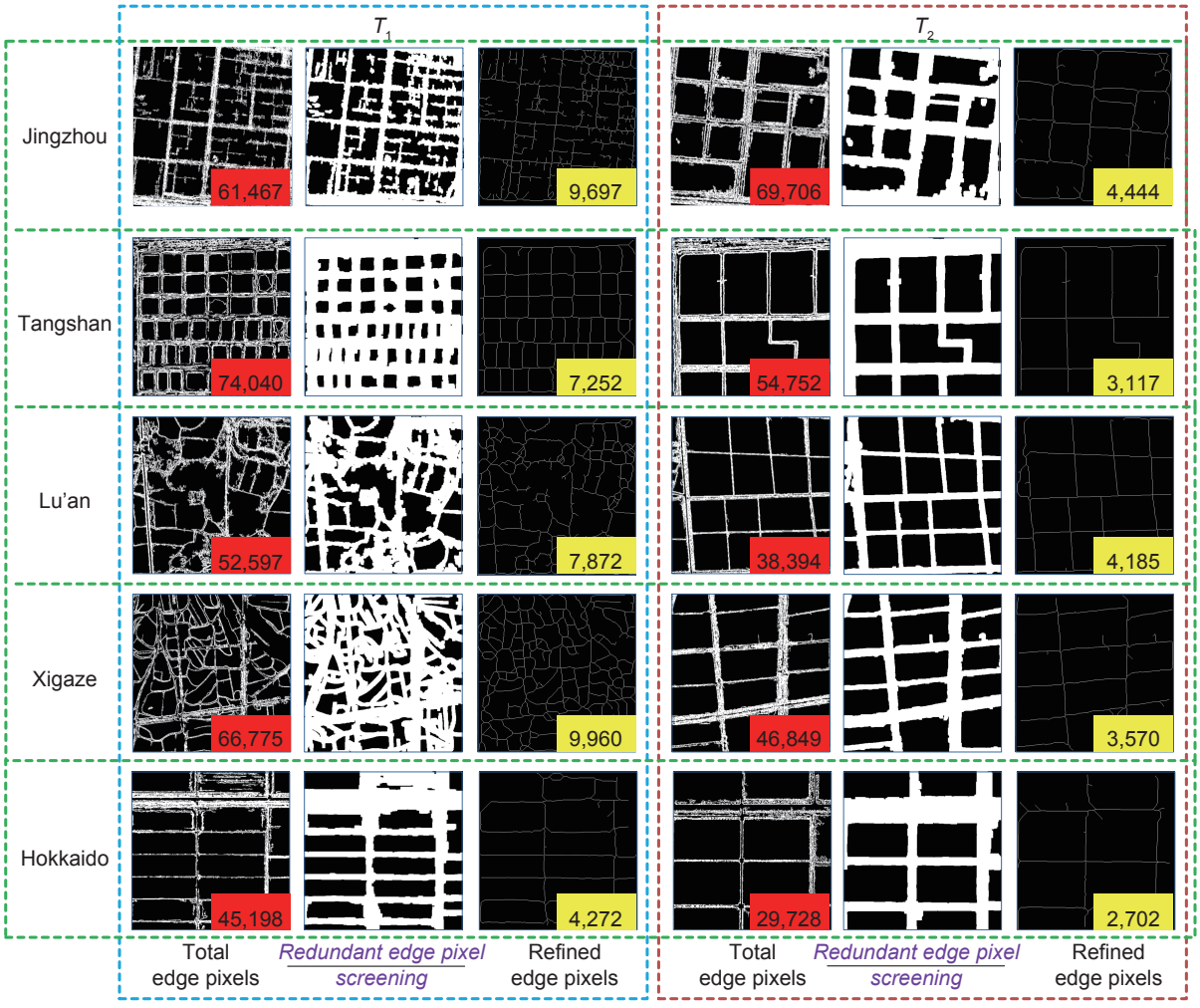


Fig. 9 Bi-temporal images redundant edge pixel screening results. The red label indicates the total edge pixels, and the yellow label indicates the refined edge pixels.

Table 2 *T*-test results of edge pixels without or with screening

Site	Without screening			With screening		
	T_1	T_2	*P*-value	T_1	T_2	*P*-value
Jingzhou	71,463.250±23,071.013	48,561.000±17,120.417	0.162	8,750.250±1,025.626	5,028.750±402.289	0.001**
Tangshan	87,511.500±17,504.286	59,379.000±9,241.989	0.059	7,494.250±635.930	4,255.750±786.735	0.001**
Lu'an	55,237.250±10,639.663	40,531.250±11,523.179	0.110	7,767.500±901.049	4,632.750±536.095	0.001**
Xigaze	57,563.750±13,181.232	38,931.500±7,053.504	0.059	9,373.000±494.075	3,709.500±433.278	<0.001***
Hokkaido	53,133±12,809.379	32,662.5±9,811.797	0.054	4,544.75±440.459	2,813±300.314	0.001**

** denotes significance at the 0.01 level, *** denotes significance at the 0.001 level.

pixels, without requiring the continuous development of full-coverage, wall-to-wall parcel maps.

4.3. Future prospects

We introduced a concept to directly detect the structural change in cropland parcel without the need to produce parcel maps. The proposed method demonstrated high performance across five East Asian study regions that have experienced LC. Several issues remain that require further research.

Firstly, the textural instability of other land types present in the figures interfered with the accuracy of change detection. The presence of land types with complex and changeable textures, such as small-range forest land, garden land, and wasteland, in proximity to cropland often resulted in numerous redundant edge pixels. This increases the total edge pixel count, reducing variability when the number of changing areas remained constant and ultimately leading to inaccurate detection. Secondly, parcel ridges were frequently obscured or blurred, complicating the perception of parcel edges and significantly affecting accurate edge pixel counting. Therefore, too sensitive or too insensitive to edge information impacted the result of structural change detection. While the proposed method allowed for a

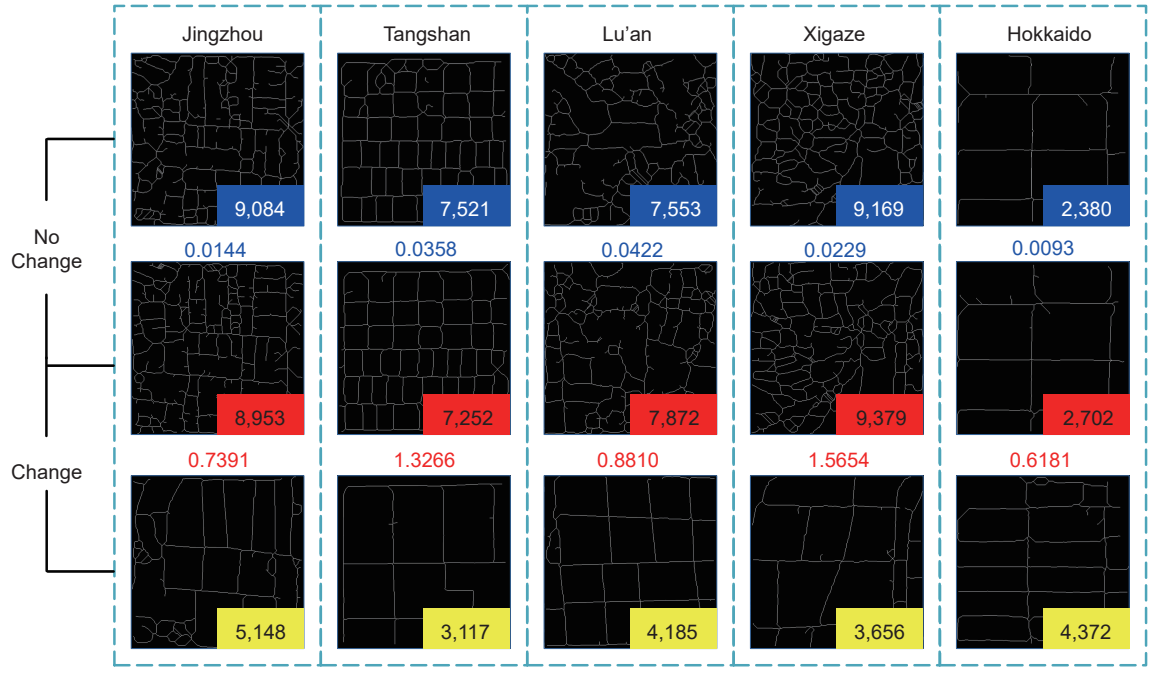


Fig. 10 The statistical result of the edge pixel fluctuation of the training set.

Table 3 Change detection accuracy assessment

Dataset	Accuracy	Precision	Recall	F1-score
All	0.8941	0.8923	0.9017	0.8970
Jingzhou	0.8725	0.8824	0.8654	0.8738
Tangshan	0.8800	0.8889	0.9091	0.8989
Lu'an	0.8567	0.8596	0.8547	0.8571
Xigaze	0.9651	0.9670	0.9462	0.9565
Hokkaido	0.9086	0.9032	0.9573	0.9295

considerable margin of error in edge detection accuracy, edge feature extraction remained central to the approach. We devised a compromise that mitigated the over-extraction of edges from other land types while accurately capturing obscured and blurred edges.Future research would explore the use of stable features to represent edge characteristics of cropland parcels, aiming for more precise detection of parcel changes and enhancing the robustness and reliability of the change detection process. Thirdly, the current sliding-window strategy outputs a binary "changed/unchanged" label per window, limiting precise localization. Although setting the window size smaller than the minimum LC operation unit and clustering adjacent positive windows provides a coarse outline of LC zones, this resolution suffices only for preliminary screening. Future work should integrate super-pixel segmentation with attention-guided edge weighting to refine window-level signals into parcel-level probability maps. Although our approach is only applied to detecting parcel changes during LC in the current paper, it can also be used in areas where land fragmentation is occurring, such as in some regions of Africa (Rufin *et al.* 2024). It is worth further upscaling its application to understand the patterns of hotspot areas of cropland consolidation versus cropland fragmentation across the globe.

5. Conclusion

This paper proposes a method for quickly identifying the consequence of cropland parcel change without producing any single complete cropland parcel maps. The method works by simple counting the number of edge pixels, which are used as the basic input in image segmentation for cropland boundary delineation. To minimize the impact of redundant edge pixels on change detection, we used connectivity component labeling, morphological expansion operations, and skeleton extraction algorithms from traditional edge detection methods. These innovations streamlined the detection of the edge pixels and ensured high detection accuracy. Experiments conducted on five typical LC applications in East Asia demonstrate the feasibility of the proposed method for detecting cropland parcel changes in different geographic and agronomic settings. These results suggest that the proposed method enables rapid detection of substantial changes in cropland parcel over large areas and facilitates accurate identification of hotspot areas of cropland parcel change. This capability provides a lightweight solution to understand the consequences of human activities on reshaping the agricultural landscape at larger scales without the need for complete wall-to-wall mapping. We advocate that the idea of structural change detection, rather than map comparison, should receive more attention in agricultural landscape studies, as it is particularly useful for monitoring the implementation of LC programs.

Acknowledgements

This work was jointly supported by the National Key Research and Development Program of China (2022YFB3903505) and the Central Public-interest Scientific Institution Basal Research

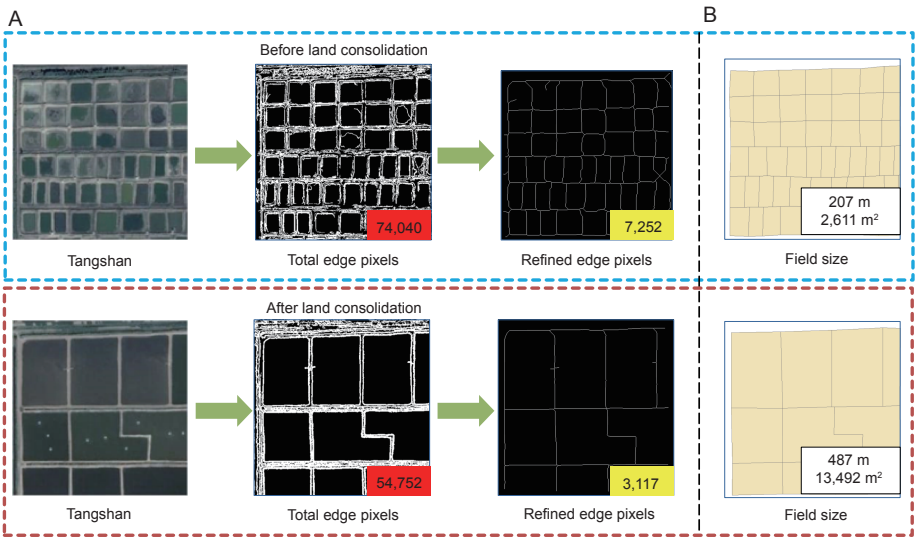


Fig. 11 Refined edge pixels related to field size. A, refined bi-temporal edge pixels after the three-stage filtering. B, external plot reference map (manually compiled, not produced by our algorithm) illustrating the inverse relationship between edge-pixel count and parcel area.

Fund, China (Y2025YC87). The Land Systems Group at IAMO offered invaluable support throughout this research. This study contributes to the Global Land Programme.

Declaration of competing interest

The authors declare that they have no conflict of interest.

Declaration of generative AI and AI-assisted technologies in the writing process

The authors declare that they did not use AI in the preparation and writing of this manuscript.

References

Abubakari Z, Van Der Molen P, Bennett R M, Kuusaana E D. 2016. Land consolidation, customary lands, and Ghana's Northern Savannah Ecological Zone: An evaluation of the possibilities and pitfalls. *Land Use Policy*, **54**, 386–398.

Al-Amin A K M A, Lowenberg-Deboer J, Franklin K, Behrendt K. 2023. Economics of field size and shape for autonomous crop machines. *Precision Agriculture*, **24**, 1738–1765.

Alcantarilla P F, Stent S, Ros G, Arroyo R, Gherardi R. 2018. Street-view change detection with deconvolutional networks. *Autonomous Robots*, **42**, 1301–1322.

Bey A, Jetimane J, Lisboa S N, Ribeiro N, Sitoe A, Meyfroidt P. 2020. Mapping smallholder and large-scale cropland dynamics with a flexible classification system and pixel-based composites in an emerging frontier of Mozambique. *Remote Sensing of Environment*, **239**, 111611.

Chen W, Sui L C, Xu Z C, Lang Y. 2012. Improved Zhang-Suen thinning algorithm in binary line drawing applications. In: *2012 International Conference on Systems and Informatics* (ICSAI 2012). IEEE, China. pp. 1947–1950.

Choi H I, Choi S W, Moon H P, Wee N S. 1997. New algorithm for medial axis transform of plane domain. *Graphical Models and Image Processing*, **59**, 463–483.

Clough Y, Kirchweger S, Kantelhardt J. 2020. Field sizes and the future of farmland biodiversity in European landscapes. *Conservation Letters*, **13**, e12752.

Du J N, Xu S C, Li J S, Duan J K, Xiao W. 2024. A novel approach for farmland size estimation in small-scale agriculture using edge counting and remote sensing. *Remote Sensing*, **16**, 2981.

Duan J K, Ren C C, Wang S T, Zhang X M, Reis S, Xu J M, Gu B J. 2021. Consolidation of agricultural land can contribute to agricultural sustainability in China. *Nature Food*, **2**, 1014–1022.

Feng W, Tian F P, Zhang Q, Zhang N, Wan L, Sun J Z. 2015. Fine-grained change detection of misaligned scenes with varied illuminations. In: *2015 IEEE International Conference on Computer Vision* (ICCV 2015). IEEE, Chile. pp. 1260–1268.

Fritz S, See L, Mccallum I, You L Z, Bun A, Moltchanova E, Duerauer M, Albrecht F, Schill C, Perger C, Havlik P, Mosnier A, Thornton P, Wood-Sichra U, Herrero M, Becker-Reshef I, Justice C, Hansen M, Gong P, Aziz S A, *et al.* 2015. Mapping global cropland and field size. *Global Change Biology*, **21**, 1980–1992.

Gao W L, Xie D Y. 2024. Pathways towards low-carbon sustainable agriculture: How farmland size affects net carbon emissions. *Climate Policy*, **24**, 1–15.

Garcia-Pedrero A, Gonzalo-Martin C, Fonseca-Luengo D, Lillo-Saavedra M. 2015. A GEOBIA methodology for fragmented agricultural landscapes. *Remote Sensing*, **7**, 767–787.

García-Pedrero A, Lillo-Saavedra M, Rodríguez-Esparragón D, Gonzalo-Martín C. 2019. Deep learning for automatic outlining agricultural parcels: Exploiting the land parcel identification system. *IEEE Access*, **7**, 158223–158236.

Gónzalez X P, Marey M F, Álvarez C J. 2007. Evaluation of productive rural land patterns with joint regard to the size, shape and dispersion of plots. *Agricultural Systems*, **92**, 52–62.

Graesser J, Ramankutty N. 2017. Detection of cropland field parcels from Landsat imagery. *Remote Sensing of Environment*, **201**, 165–180.

Gu T C, Chen W X, Liang J L, Pan S P, Ye X Y. 2023. Identifying the driving forces of cultivated land fragmentation in China. *Environmental Science and Pollution Research*, **30**, 105275–105292.

He L F, Ren X W, Gao Q H, Zhao X, Yao B, Chao Y Y. 2017. The connected-component labeling problem: A review of state-of-the-art algorithms. *Pattern Recognition*, **70**, 25–43.

Hemond O, Butsic V, Moanga D, Wartenberg A C. 2023. Farm consolidation and turnover dynamics linked to increased crop diversity and higher agricultural input use. *Agricultural Systems*, **210**, 103708.

Hendricks A, Lisec A. 2014. Land consolidation for large-scale infrastructure projects in Germany. *Geodetski Vestnik*, **58**, 46–68.

Huang R, Wang R F, Zhang Y X, Xing Y, Fan W, Yung K L. 2022. Selecting change image for efficient change detection. *IET Signal Processing*, **16**, 327–339.

Huang R, Zhou M, Zhao Q, Zou Y B. 2020. Change detection with absolute difference of multiscale deep features. *Neurocomputing*, **418**, 102–113.

Hussain M, Chen D M, Cheng A, Wei H, Stanley D. 2013. Change

detection from remotely sensed images: From pixel-based to object-based approaches. *ISPRS Journal of Photogrammetry and Remote Sensing*, **80**, 91–106.
Jänicke C, Wesemeyer M, Chiarella C, Lakes T, Levers C, Meyfroidt P, Müller D, Pratzer M, Rufin P. 2024. Can we estimate farm size from field size? An empirical investigation of the field size to farm size relationship. *Agricultural Systems*, **220**, 104088.
Janulevičius A, Šarauskis E, Čiplienė A, Juostas A. 2019. Estimation of farm tractor performance as a function of time efficiency during ploughing in fields of different sizes. *Biosystems Engineering*, **179**, 80–93.
Jiang Y F, Tang Y T, Long H L, Deng W. 2022. Land consolidation: A comparative research between Europe and China. *Land Use Policy*, **112**, 105790.
Kong W B, Chen J Z, Song Y B, Fang Z Q, Yang X F, Zhang H Y. 2023. Sobel edge detection algorithm with adaptive threshold based on improved genetic algorithm for image processing. *International Journal of Advanced Computer Science and Applications*, **14**, 557–562.
Kwinta A, Gniadek J. 2017. The description of parcel geometry and its application in terms of land consolidation planning. *Computers and Electronics in Agriculture*, **136**, 117–124.
Lam L, Lee S W, Suen C Y. 1992. Thinning methodologies — a comprehensive survey. *IEEE Transactions on Pattern Analysis and Machine Intelligence*, **14**, 869–885.
Langeveld H, Röling N. 2006. *Changing European Farming Systems for a Better Future*: *New Visions for Rural Areas*. Wageningen Academic Publishers, Wageningen.
Lee T C, Kashyap R L, Chu C N. 1994. Building skeleton models via 3-D medial surface axis thinning algorithms. *CVGIP: Graphical Models and Image Processing*, **56**, 462–478.
Li M M, Lu C W, Lin M J, Xiu X L, Long J, Wang X Q. 2025. Extracting vectorized agricultural parcels from high-resolution satellite images using a Point-Line-Region interactive multitask model. *Computers and Electronics in Agriculture*, **231**, 109953.
Li S N, Pu J W, Deng X D. 2025b. Agricultural land use transition under multidimensional topographical gradients and its impact on ecosystem service interactions. *Journal of Integrative Agriculture*, **24**, 3222–3241.
Liu S C, Marinelli D, Bruzzone L, Bovolo F. 2019. A review of change detection in multitemporal hyperspectral images: Current techniques, applications, and challenges. *IEEE Geoscience and Remote Sensing Magazine*, **7**, 140–158.
Lowder S K, Sánchez M V, Bertini R. 2021. Which farms feed the world and has farmland become more concentrated? *World Development*, **142**, 105455.
Meng X. 2018. Digital image processing technology based on MATLAB. In: *Proceedings of the 4th International Conference on Virtual Reality* (ICVR 2018). Association for Computing Machinery, Hong Kong. pp. 79–82.
Noack F, Larsen A, Kamp J, Levers C. 2022. A bird's eye view of farm size and biodiversity: The ecological legacy of the iron curtain. *American Journal of Agricultural Economics*, **104**, 1460–1484.
Persello C, Tolpekin V A, Bergado J R, De By R A. 2019. Delineation of agricultural fields in smallholder farms from satellite images using fully convolutional networks and combinatorial grouping. *Remote Sensing of Environment*, **231**, 111253.
Qian F K, Chi Y R, Lal R, Lorenz K. 2020. Spatio-temporal characteristics of cultivated land fragmentation in different landform areas with a case study in Northeast China. *Ecosystem Health and Sustainability*, **6**, 12.
Qu Y D, Cui C S, Chen S B, Li J Q. 2005. A fast subpixel edge detection method using Sobel–Zernike moments operator. *Image and Vision Computing*, **23**, 11–17.
Ranjan R, Avasthi V. 2023. Edge detection using guided Sobel image filtering. *Wireless Personal Communications*, **132**, 651–677.
Rogers S, Wilmsen B, Han X, Wang Z J H, Duan Y F, He J, Li J, Lin W L, Wong C. 2021. Scaling up agriculture? The dynamics of land transfer in inland China. *World Development*, **146**, 105563.
Rosenfeld A, Pfaltz J L. 1966. Sequential operations in digital picture processing. *Journal of the ACM*, **13**, 471–494.
Rufin P, Wang S, Lisboa S N, Hemmerling J, Tulbure M G, Meyfroidt P. 2024. Taking it further: Leveraging pseudo-labels for field delineation across label-scarce smallholder regions. *International Journal of Applied Earth Observation and Geoinformation*, **134**, 104149.
Shi W Z, Zhang M, Zhang R, Chen S X, Zhan Z. 2020. Change detection based on artificial intelligence: State-of-the-art and challenges. *Remote Sensing*, **12**, 1688.
Singh A. 1989. Review article digital change detection techniques using remotely-sensed data. *International Journal of Remote Sensing*, **10**, 989–1003.
Al Smadi P T, Zoubi S. 2021. Modern technology for image processing and computer vision — A review. *Journal of Advanced Sciences and Engineering Technologies*, **1**, 17–23.
Sobel I. 1978. Neighborhood coding of binary images for fast contour following and general binary array processing. *Computer Graphics and Image Processing*, **8**, 127–135.
Sun H R, Wei Z J, Yu W G, Yang G X, She J N, Zheng H B, Jiang C Y, Yao X, Zhu Y, Cao W X, Cheng T, Ali I. 2025. SIDEST: A sample-free framework for crop field boundary delineation by integrating super-resolution image reconstruction and dual edge-corrected Segment Anything model. *Computers and Electronics in Agriculture*, **230**, 109897.
Sun Z D, Zhong Y F, Wang X Y, Zhang L P. 2024. Identifying cropland non-agriculturalization with high representational consistency from bi-temporal high-resolution remote sensing images: From benchmark datasets to real-world application. *ISPRS Journal of Photogrammetry and Remote Sensing*, **212**, 454–474.
Tong X, Ren A F, Zhang H F, Ruan H, Luo M. 2011. Edge detection based on genetic algorithm and sobel operator in image. In: *International Conference on Graphic and Image Processing* (ICGIP 2011). SPIE, Egypt. pp. 828572.
Walczyk R, Armitage A, Binnie D. 2010. Comparative study on connected component labeling algorithms for embedded video processing systems. In: *International Conference on Image Processing*, *Computer Vision*, *& Pattern Recognition* (IPCV 2010). CSREA, USA. pp. 853–859.
Wang S Y, Zhou Y N, Yang X Z, Feng L, Wu T J, Luo J C. 2023. BSNet: Boundary-semantic-fusion network for farmland parcel mapping in high-resolution satellite images. *Computers and Electronics in Agriculture*, **206**, 107683.
Wang X Q, Shi W J, Yu Q Y, Deng X Z, Zuo L J, Shi X L, Wang M L, Li J. 2025. Well-facilitated farmland improves nitrogen use efficiency and reduces environmental impacts in the Huang-Huai-Hai Region, China. *Journal of Integrative Agriculture*, **24**, 3264–3281.
Xu L, Ming D P, Du T Y, Chen Y Y, Dong D H, Zhou C H. 2022. Delineation of cultivated land parcels based on deep convolutional networks and geographical thematic scene division of remotely sensed images. *Computers and Electronics in Agriculture*, **192**, 106611.
Xu Y Y, Zhu Z H, Guo M Q, Huang Y. 2024. Multiscale edge-guided network for accurate cultivated land parcel boundary extraction from remote sensing images. *IEEE Transactions on Geoscience and Remote Sensing*, **62**, 1–20.
Yang Y B, Wilson L T, Wang J. 2014. Reconciling field size distributions of the US NASS (National Agricultural Statistics Service) cropland data. *Computers and Electronics in Agriculture*, **109**, 232–246.
Yu Q Y, Hu Q, Wu H, Wu W B. 2025. View from above: Farmland infrastructure and its impacts on agricultural landscapes. *The Innovation Geoscience*, **3**, 100107.
Zhang T Y, Suen C Y. 1984. A fast parallel algorithm for thinning digital patterns. *Communications of the ACM*, **27**, 236–239.
Zhang Z X, Jiang H W, Pang S Y, Hu X Y. 2022. Review and prospect in change detection of multi-temporal remote sensing images. *Acta Geodetica et Cartographica Sinica*, **51**, 1091–1107. (in Chinese)

Executive Editor-in-Chief Keke Yi
Managing Editor Lujuan Sun